Proc. Natl. Acad. Sci. USA
Vol. 93, pp. 8648–8653, August 1996
Neurobiology

Probing the pore region of recombinant *N*-methyl-D-aspartate channels using external and internal magnesium block

(glutamate receptor/mutagenesis/ionic channel)

JÜRGEN KUPPER, PHILIPPE ASCHER, AND JACQUES NEYTON†

Laboratoire de Neurobiologie, Centre National de la Recherche Scientifique Unité de Recherche Associée 1857, Ecole Normale Supérieure, 46, rue d'Ulm, 75005 Paris, France

Communicated by Clay M. Armstrong, University of Pennsylvania Medical Center, Philadelphia, PA, April 29, 1996 (received for review January 31, 1996)

ABSTRACT **Mg^{2+} ions block *N*-methyl-D-aspartate (NMDA) channels by entering the pore from either the extracellular or the cytoplasmic side of the membrane in a voltage-dependent manner. We have used these two different block phenomena to probe the structure of the subunits forming NMDA channels. We have made several amino acid substitutions downstream of the Q/R/N site in the TMII region of both NR1 and NR2A subunits. Mutant NR1 subunits were coexpressed with wild-type NR2A subunits and vice versa in *Xenopus* oocytes. We found that individually mutating the first two amino acid residues downstream to the Q/R/N site affects mostly the block by external Mg^{2+}. Mutations of residues five to seven positions downstream of the Q/R/N site do not influence the external Mg^{2+} block, but clearly influence the block by internal Mg^{2+}. These data add support to the hypothesis that there are two separate binding sites for external and internal Mg^{2+} block. They also indicate that the C-terminal end of TMII contributes to the inner vestibule of the pore of NMDA channels and thus provide additional evidence that TMII forms a loop that reemerges toward the cytoplasmic side of the membrane.**

N-methyl-D-aspartate (NMDA) receptors form cation selective ion channels at excitatory synapses and can be distinguished from other glutamate-gated ion channels by their pharmacological and biophysical properties (1). The voltage dependence of the NMDA receptor channel, which is thought to play an important role in many physiological and pathophysiological processes, results from an extracellular Mg^{2+} block (2, 3), which increases markedly with hyperpolarization due to the binding of Mg^{2+} deep inside the pore (4, 5). Mg^{2+} ions can also block the NMDA channel from the cytoplasmic surface (6). Like the external Mg^{2+} block, the internal Mg^{2+} block is voltage dependent, but it increases with depolarization and the unblocking rate of internal Mg^{2+} is two orders of magnitude faster than that of external Mg^{2+}. It has been proposed that external and internal Mg^{2+} bind to two different blocking sites within the channel pore (6, 7).

The genes coding for the subunits of the NMDA receptor have recently been cloned, offering new opportunities for structure function studies (8–10). Functional channels are composed of the NR1 subunit and one or more members of the NR2 family. Site-directed mutagenesis rapidly identified an asparagine residue (N) as playing a key role in the external Mg^{2+} block (11–13). The position of this residue, which is occupied in non-NMDA glutamate-activated channels by either a glutamine (Q) or an arginine (R) controlling the Ca^{2+} permeability, has been labeled Q/R/N site. It is located in a relatively hydrophobic segment referred to as TMII based on the initial assumption that it was the second transmembrane segment. In contrast, the region involved in the control of the block by internal Mg^{2+} is unknown.

Recently, a series of biochemical studies (14–17) have suggested that, instead of traversing the membrane, the region labeled TMII forms a loop, dipping in and out of the membrane from the internal side. Such pore loops have become a common structural motif in the case of the voltage-gated ion channels since they were first proposed for the *Shaker* potassium channel by Yellen *et al.* (18). They used tetraethylammonium (TEA), known to block potassium channels from both sides of the membrane, to probe the structure of a 20 amino acid stretch in the linker between the membrane spanning domains S5 and S6. Mutations on both ends of this "P region" were found to affect only the block by external TEA, whereas a mutation in the center of the P region selectively affected the internal TEA block.

In the present study, we have used a similar approach to test whether the mutation of certain amino acid residues downstream of the Q/R/N site affects differentially the blocks produced by internal and external Mg^{2+}. Again, the results suggest that permeation in the channel involves a pore loop.

MATERIALS AND METHODS

Expression of cDNA in *Xenopus* Oocytes. The NMDA subunit cDNAs coding for NR1 (pN60, ref. 8, a gift from S. Nakanishi, Kyoto University, Kyoto) and NR2A (NR2A, ref. 9, a gift from P. Seeburg, Center for Molecular Biology, Heidelberg) were subcloned in the pcDNA3 vector (Invitrogen). To speed up and enhance the expression of recombinant channels in *Xenopus* oocytes after nuclear injection of cDNA, a stretch of 36 bases corresponding to the 5′ untranslated region of the alfalfa mosaic virus (19) was inserted between the cytomegalovirus promoter and the pcDNA3 polylinker, and most of the 5′ untranslated regions and the 3′ untranslated regions of the original clones (pN60 and NR2A) were removed. Site-directed mutagenesis was carried out according to a method modified from Kunkel (20). We sequenced across the TMII region to verify the mutations using the Sequenase kit (Stratagene). For each mutation, we functionally tested at least two independent colonies to verify that the observed phenotype results from the introduced mutation and not from a stray mutation. To designate individual mutant channels, we used a nomenclature based on the position of the altered amino acid in relation to the Q/R/N site. Fig. 1 shows the C-terminal amino acid sequences of the TMII region of NR1 and NR2A subunits and the mutations analyzed in the present study.

Preparation of oocytes and nuclear injection of cDNAs coding for wild-type and mutant NMDA channels were carried

The publication costs of this article were defrayed in part by page charge payment. This article must therefore be hereby marked "*advertisement*" in accordance with 18 U.S.C. §1734 solely to indicate this fact.

Abbreviations: NMDA, *N*-methyl-D-aspartate; UF, unblocked fraction; *I–V*, current–voltage.

†To whom reprint requests should be addressed.

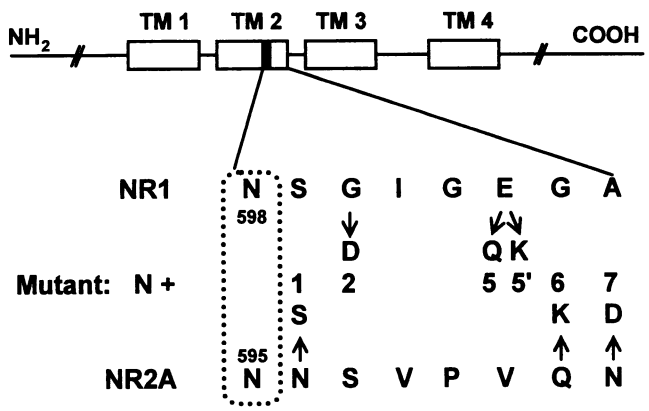

FIG. 1. Nomenclature of mutant NMDA channels. Amino acid sequences (single letter code) of the C-terminal portion of the second hydrophobic domain of the NR1 (*Upper*) and NR2A (*Lower*) subunits of NMDA channels. The Q/R/N site is indicated by the dashed box. The numbers used to designate each of the mutations are indicated in the line labelled Mutant (center). Above or below each number the single amino acid mutation is indicated. Thus, mutant N+1 represents the NR2A N596S mutation and N+5′ represents the NR1 E603K mutation.

out as described (21). Approximately 80 pg of NR1 and NR2A cDNAs mixed at a ratio of 1:3 was injected into each oocyte. Mutant NR1 subunits were coexpressed with wild-type NR2A subunits and vice versa. As early as 1 day after injection, we measured glutamate-activated whole cell currents between 1 and 5 μA (−80 mV, no external Ca^{2+}).

Recording Conditions and Data Analysis. *Internal Mg^{2+} block.* Li-Smerin and Johnson (22) have obtained evidence that internal Mg^{2+} has two effects on NMDA currents: (*i*) it reduces the single channel conductance and (*ii*) it prolongs the opening of the channels. Therefore, to avoid the superposition of the two effects observed at the whole-cell level, the analysis of the internal Mg^{2+} block was done at the single channel level. Moreover, the outside-out patch-clamp configuration was chosen to be able to positively identify NMDA channels by shifting the patch electrode in and out of a glutamate containing solution.

Patch pipettes, pulled from hard borosilicate glass (Hilgenberg, Malsfeld, Germany), had a resistance of about 5 MΩ and were filled with a control solution containing 140 mM CsCl, 10 mM Hepes, and 10 mM bis(2-aminophenoxy)ethane-*N*,*N*,*N*′,*N*′-tetra-acetate (BAPTA; pH 7.2 adjusted with CsOH). For the Mg^{2+}-containing solution, 5.14 mM $MgCl_2$ was added to the control solution to yield a free Mg^{2+} concentration of 4 mM as calculated with the Chelator program kindly provided by T. Schoenmakers (23). Recordings were made 1–5 days after cDNA injection. Outside-out patches were formed from oocytes superfused with extracellular solution containing 140 mM NaCl, 2.8 mM KCl, 1 mM $CaCl_2$, and 10 mM Hepes (pH 7.2 adjusted with NaOH). After obtaining a stable patch, the pipette was moved into the stream of a double-barrel perfusion system (24). Both the control solution and the glutamate solution (10 μM glutamate) contained 10 μM glycine and lacked Ca^{2+} to minimize activation of endogenous Ca^{2+}-activated conductances. While the patch was perfused with the glutamate solution, the membrane was brought from a holding potential of −60 mV to test potentials ranging from −80 mV to +80 mV in steps of 10 mV or 20 mV.

Single channel currents were recorded using an Axopatch 200A amplifier (Axon Instruments, Foster City, CA), low-pass filtered at 2 kHz with an 8-pole Bessel filter and sampled at 5 kHz. Amplitude histograms were built from a minimum of 100 transitions detected with a 50% threshold crossing routine and fitted by Gaussian curves using the STRATHCLYDE ELECTROPHYSIOLOGICAL software package (John Dempster, University of Strathclyde).

We quantified the internal Mg^{2+} block by determining at +60 mV the unblocked fraction (UF), which is the ratio of the mean channel current in the presence of 4 mM Mg^{2+} (i_{Mg}) over that in the absence of Mg^{2+} (i_0). We assumed that the single channel mean amplitudes obtained from at least three different patches for each mutant channel were normally distributed. This then allows the use of a Student's *t* test (25) to evaluate whether the differences between the ratios of the mean values of the single channel current were significant. The variance of the ratio is

$$s^2(UF) = \left(\frac{\bar{i}_{Mg}}{\bar{i}_0}\right)^2 * \left(\frac{s^2_{Mg}}{n_{Mg} * \bar{i}^2_{Mg}} + \frac{s^2_0}{n_0 * \bar{i}^2_o}\right)$$

and

$$t = \frac{UF_{WT} - UF_{Mutant}}{\sqrt{s^2(UF_{WT}) + s^2(UF_{Mutant})}}.$$

External Mg^{2+} block was analyzed in whole oocyte currents in two electrodes voltage clamp experiments. Voltage and current electrodes were filled with 3 M KCl and had resistances of 0.5–1.5 MΩ. The currents were recorded during voltage ramps (−150 mV to +100 mV within 2 sec). Between ramps, the oocyte was kept at a holding potential of −60 mV. All extracellular solutions contained 100 mM NaCl, 2.5 mM KCl, 10 mM Hepes, and 0.1 mM EGTA (pH 7.6 adjusted with NaOH). Ca^{2+} was eliminated from the extracellular solutions to suppress the contamination of the measured currents by Ca^{2+}-activated endogenous currents (26), which is particularly important for NMDA current measurements at potentials above 0 mV. Mg^{2+}-free solutions (supplemented with 0.1 mM EDTA) and low Mg^{2+} solutions were only applied briefly because, upon complete removal of divalent cations, a slow but large endogenous cationic current develops in the oocyte (27). To avoid the development of this current, each low Mg^{2+} measurement was followed by a period of at least 3 min in a solution containing 1 mM Mg^{2+}. The glutamate-induced current was calculated as the difference between the current recorded 10 sec after the application of the two coagonists (glutamate and glycine, both at 100 μM) and the current recorded 5 sec before the agonist application.

Macroscopic NMDA currents were sampled and filtered at 200 Hz and recorded using a Warner Instruments (Hamden, CT) model OC-725 amplifier. Digitized traces were acquired using pClamp V6.0 (Axon Instruments).

All experiments were carried out at room temperature (20–22°C).

RESULTS

Internal Mg^{2+} Block of Wild-Type NMDA Channels. As illustrated in Fig. 2*A*, the internal Mg^{2+} block, previously described for native NMDA channels (6), is conserved in recombinant (NR1–NR2A) NMDA receptors. The single channel currents observed at positive potentials in a patch exposed to 4 mM Mg^{2+} are smaller than those observed in another patch exposed to a Mg^{2+}-free solution and do not display detectable flickering, suggesting that the block is too fast to be resolved under our recording conditions. The current–voltage (*I–V*) curve obtained in the presence of 4 mM internal Mg^{2+} (Fig. 2*B*) is characteristic for a voltage dependent block. At positive potentials, the single channel current reaches a maximum (at about +40 mV) and then decreases again.

Internal Mg^{2+} Block of Mutant NMDA Receptors. In our search for amino acid residues involved in the internal Mg^{2+}

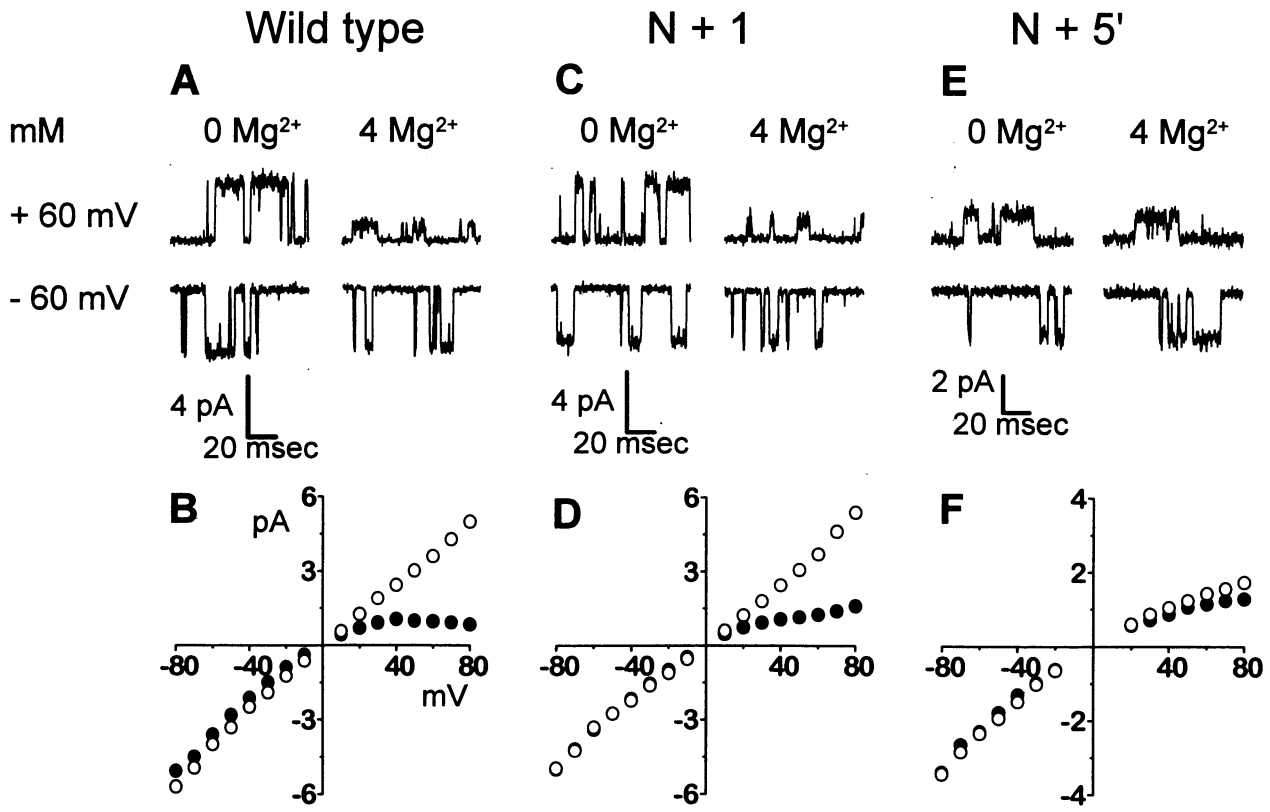

FIG. 2. Internal Mg^{2+} block of wild-type and mutant NMDA channels. (*A*, *C*, and *E*) Representative single channel recordings of the wild-type, N+1, and N+5′ mutant channels in the absence and presence of 4 mM internal Mg^{2+}. Each pair of records was obtained in a different outside-out patch. Holding potentials are +60 mV (upper traces) and −60 mV (lower traces). (*B*, *D*, and *F*) Corresponding single channel *I–V* relations in the absence (○) and presence (●) of 4 mM internal Mg^{2+}.

blocking site and, in light of the revised membrane topology of NMDA receptors, obvious candidates were residue NR1 E603 (28) and polar residues NR2A Q601 and NR2A N602 located in almost homologous positions. At these positions, we introduced amino acid substitutions that changed the charge of the residue and expected a dramatic effect on the internal Mg^{2+} block. On the other hand, if internal and external Mg^{2+} were to block NMDA channels by binding to two separate sites, we expected that mutations at the Q/R/N site would not affect the internal Mg^{2+} block. With this in mind, we produced several mutants at the Q/R/N sites in both the NR1 and the NR2A subunits. Unfortunately, those mutant channels have very pronounced subconductance states, which makes them unsuitable for internal Mg^{2+} block studies. We therefore chose two other mutations near the Q/R/N site [N+1 (NR2A N596S); N+2 (NR1 G600D)] that do not display stable subconductance states. It has previously been mentioned that the N+1 mutation strongly affects the external Mg^{2+} block (29).

Fig. 2 *C–F* shows single channel recordings and the corresponding *I–V* relations of the two mutants (N+1 and N+5′) displaying the most extreme phenotypes regarding the internal Mg^{2+} block. For the N+1 mutant, both the single channel conductance and the internal Mg^{2+} block are quite similar to those of the wild type (compare Fig. 2 *C* and *D* with *A* and *B*). The only difference is that at high positive potentials, and in the presence of Mg^{2+}, the single channel current, which in the wild-type channel tends to decrease, keeps increasing in the mutant. In strong contrast, the N+5′ mutant channel (NR1 E603K) is very different from the wild-type channel: it has a lower single channel conductance, it exhibits a stronger inward rectification even in the absence of internal Mg^{2+}, and, finally, it appears to be much less sensitive to the block by internal Mg^{2+} (Fig. 2 *E* and *F*).

The upturn of the *I–V* curve observed in some mutants is likely to indicate that, in some channels, Mg^{2+} ions can permeate (escape) through the channel (see *Discussion*) and the full description of the block would require the evaluation of at least the three rates of Mg^{2+} blocking, Mg^{2+} unblocking, and Mg^{2+} permeation (30). However, we considered that, to a first approximation, it was sufficient to characterize the block at a potential (+60 mV) at which the escape phenomenon was relatively limited, even in those mutants, like N+1, where this phenomenon is most detectable. As shown in Table 1, the UF of the current of four of the six mutations is significantly higher than that of the wild-type channel, indicating that in these channel mutants the internal Mg^{2+} block is reduced. The sequence of block potency is (N+2, wild type, N+1) > N+6 > N+5 > N+7 > N+5′. However, even mutations N+1 and N+2 showing an UF value close to the wild-type UF value have an altered internal Mg^{2+} block better revealed at very positive potentials (e.g., see Fig. 2*D*). Note also that the single channel conductance is strongly reduced in three of the six mutations (N+2, N+5′, and N+7).

External Mg^{2+} Block of Wild-Type and Mutant NMDA Receptor Channels. Glutamate-activated currents in recombinant NMDA receptor channels are blocked by external Mg^{2+} (8, 9) in a way similar to what has been observed for native NMDA receptors (refs. 2, 3, and 5; see also Fig. 3*A*) and this block is strongly affected by mutations in the Q/R/N site of the TMII region (10–12). As can be seen in Fig. 3*B*, this block is also dramatically weakened in the N+1 mutant. In the hyperpolarized range, when the potential is made increasingly negative, the *I–V* relation in the presence of external Mg^{2+} initially bends upward, but then turns back downward. Thus, the escape observed for internal Mg^{2+} in this mutant channel is also observed for externally applied Mg^{2+} and induces, at all

Table 1. Internal and external Mg^{2+} block of wild-type and mutant NMDA receptors

Mutant	Channel	Internal Mg^{2+} block: i_{+60mV}, 0 Mg^{2+}, pA	Internal Mg^{2+} block: i_{+60mV}, 4 Mg^{2+}, pA	Internal Mg^{2+} block: UF	External Mg^{2+} block IC_{50} at −50 mV, μM
WT	R1 + 2A	3.70 ± 0.21 (5)	1.15 ± 0.21 (5)	0.31	64 ± 6
N+1	R1 + 2A N596S	4.11 ± 0.33 (4)	1.29 ± 0.05 (5)	0.31	647 ± 75
N+2	R1 G600D + 2A	1.68 ± 0.17 (4)	0.44 ± 0.09 (4)	0.26	179 ± 5
N+5	R1 E603Q + 2A	3.29 ± 0.08 (4)	1.70 ± 0.05 (4)	0.52*	73 ± 15
N+5′	R1 E603K + 2A	1.45 ± 0.20 (5)	1.07 ± 0.13 (6)	0.74*	79 ± 5
N+6	R1 + 2A Q601K	3.12 ± 0.19 (3)	1.24 ± 0.11 (3)	0.40**	88 ± 9
N+7	R1 + 2A N602D	1.23 ± 0.23 (3)	0.72 ± 0.04 (4)	0.58*	92 ± 8

The internal Mg^{2+} block potency has been measured at +60mV for each channel construct as the UF, which is the ratio of the mean single channel current in the presence of 4 mM internal Mg^{2+} [i_{+60mV}, 4 Mg^{2+} given as mean ± SD (n = number of patches)] over that in the absence of internal Mg^{2+} (i_{+60mV}, 0 Mg^{2+}). To test whether the UF value of a mutant was significantly different from the wild-type UF value, we used a modified Student's t test as described. To rank the mutants on a scale of decreasing internal block potency (see text), we also verified that the UF values of N+5, N+5′, and N+6 are significantly different ($P > 0.975$) from each other. IC_{50} values of external Mg^{2+} block at −50 mV were estimated as described in the legend of Fig. 4. The last column gives the resulting best fit values ± χ^2.
*$P > 0.99$; **$P > 0.95$.

voltages, a strong decrease in the potency of the block (see also Fig. 4*A*).

In contrast, the double charge mutation five positions C terminal to the Q/R/N site (N+5′) has virtually no effect on the external Mg^{2+} block induced at hyperpolarized potentials (compare Fig. 3 *C* with *A*; see also Fig. 4*A*). At depolarized potentials, the whole cell *I–V* relation of the N+5′ mutant displays clearly less inward rectification than that of the wild type. The inward rectification in the wild-type channel is likely to result from the block of NMDA channels by cytoplasmic Mg^{2+} present inside *Xenopus* oocytes. The attenuation of this inward rectification in the N+5′ mutant is expected since the mutant channels have a reduced block by internal Mg^{2+} (Fig. 2 *E* and *F*).

We evaluated the external Mg^{2+} block of the six mutant NMDA channels by measuring both its IC_{50} values (at −50 mV) and its voltage dependence (between −150 mV and +100 mV). The values of the IC_{50} are listed in Table 1, column 6 (see also Fig. 4*A*). To characterize the voltage dependence of the external Mg^{2+} block, we plotted the ratio of the glutamate-induced current measured during a voltage ramp in the presence of 100 μM Mg^{2+} over the current in Mg^{2+}-free solution (Fig. 4*B*). Whereas the block by external Mg^{2+} was practically unchanged over the full voltage range in the mutant channels N+5, N+5′, N+6, and N+7, its voltage dependence clearly decreased in N+1 and N+2 mutants at intermediate hyperpolarized potentials (−50 mV to −100 mV), and even acquired a reversed polarity with stronger hyperpolarizations ($V < -100$ mV). These data demonstrate that while mutations downstream but close to the Q/R/N site strongly affect the block by external Mg^{2+}, mutations placed further down (more than four residues away) have virtually no effect.

DISCUSSION

We have tested the topology of the NMDA channel by extending to the TMII segment of the NMDA channel subunits the approach used by Yellen *et al.* (18) in their identification of the "P loop" of K channels. This extension was generally successful: the mutations close to the Q/R/N site affected mostly the external Mg^{2+} block, whereas the block by internal Mg^{2+} was most affected by mutations five to seven positions downstream from the Q/R/N site. These data are in agreement with the hypothesis (14–17) that the TMII segment forms a loop, and strongly suggest that the mutated segment (from Q/R/N down) points toward the cytoplasm. Beyond these conclusions, the data also allow us to advance some speculations about the energy profiles for Mg^{2+} inside the NMDA channel.

The majority of the mutations that we made involved a change in electrical charge, and one of our expectations was that such a change, if effected close to a Mg^{2+} binding site, would produce a marked effect on Mg^{2+} block. This expectation was reinforced by the fact that, although the number of subunits in a NMDA receptor is unknown, it is highly probable that each subunit exists in more than one element in each

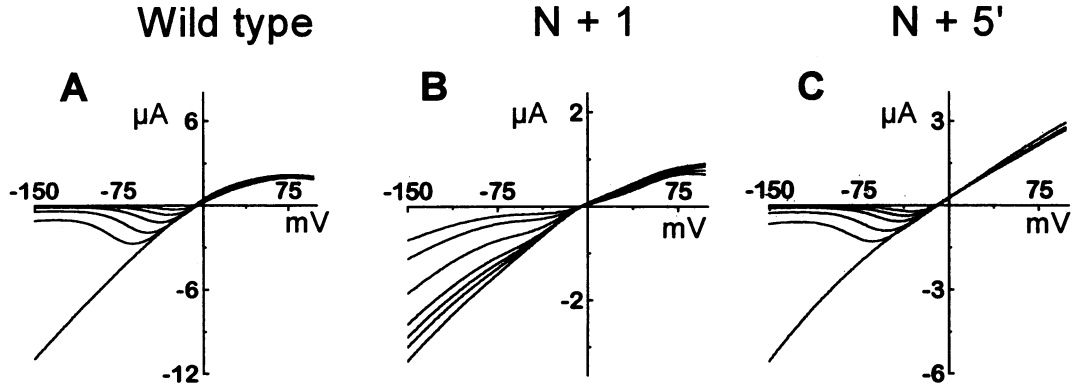

FIG. 3. External Mg^{2+} block of wild-type and mutant NMDA channels. Representative whole oocyte *I–V* curves for wild-type (*A*), N+1 (*B*), and N+5′ (*C*) mutant channels at different concentrations of external Mg^{2+} (0, 10, 30, 100, 300, and 1000 μM, with an additional 3 mM Mg^{2+} concentration in *B*).

receptor. It was therefore somewhat surprising to find that the alteration of the internal Mg^{2+} block was rather mild, even for the most effective of the "deep" mutations. The block was evaluated by determining the unblocked fraction of the current, UF, at +60 mV. This value is related to the value of the apparent dissociation constant of the binding, K_{app}, by

$$UF = \frac{i_{Mg^{2+}}}{i_{control}} = \frac{K_{app}}{K_{app} + [Mg^{2+}]}.$$

Solving for K_{app} yields a value of 1.8 mM for the wild-type NMDA channel, a value very close to 1.9 mM, which was the K_{app} value obtained by Li-Smerin and Johnson in their study on native channels in cell cultures (7). For the most severely affected mutant channel (N+5′), K_{app} is 11.4 mM. This rather small change in the K_{app} makes it unlikely that the glutamate at position 603 of the NR1 subunit directly participates in the binding site for internal Mg^{2+}. It is more likely that the reduced internal Mg^{2+} block in the N+5′ (and in N+5) channel mutants is due to remote electrostatic interactions. As can be seen in Fig. 2*E*, the elementary conductance of N+5′ mutant channels is smaller than that of wild-type channels and the single channel *I–V* relation of N+5′ in the absence of internal Mg^{2+} rectifies strongly inward (Fig. 2*F*). This behavior is that of a channel in which positive charges have been added in or close to the inner mouth (31–33). Such positive surface charges are expected to induce inward rectification, but also to decrease the potency of positively charged internal blockers (33). Thus, the interpretation also predicts the progressive change in K_{app} associated with a change of the charge from −1 (wild type) to 0 (N+5) to +1 (N+5′). Note that the fact that the mutations at position N+5 modify the channel elementary properties (reduced conductance and inward rectification) even in the absence of Mg^{2+} provides additional evidence that the residue at this position must face the cytoplasm.

The observed effects are not all explained by local changes of surface charge. For example, the UF value is smaller in the N+6 than in the N+5 mutant despite that in both cases the change in the charge introduced by the mutations is the same. This might be explained by assuming either that the two types of subunit do not contribute evenly to the Mg^{2+} binding site or that the residues are not at the same distance from Mg^{2+} blocking site. More puzzling is the case of the N+7 mutant, in which the addition of a negative charge appears to reduce the internal Mg^{2+} block, i.e., to act in the same direction as the addition of one or two positive charges in the mutants N+5, N+6, and N+5′. However, it should be noted that the N+7 mutant channels have a much smaller single channel conductance than the wild-type channels. Residue NR2A N602 may be not exposed to the aqueous pore and, as a consequence, a charge mutation might induce profound structural rearrangements in the channel protein.

The case of the mutation near the Q/R/N site in which there was no change in charge (N+1) appears different from that of the other mutants discussed above. In this mutant, the block by internal Mg^{2+} does not appear markedly modified below +60 mV, but at more positive potentials the upturn in the *I–V* relation indicates the presence of a marked "escape." A symmetrical behavior is observed in the negative potential range in the presence of external Mg^{2+}: the downturn of the *I–V* relation occurs at much less negative potentials in the mutant than in the wild type, where it was first described by Mayer and Westbrook (34). These results strongly suggest that the main effect of the mutation is to increase the permeation rate for Mg^{2+} in both directions, possibly by lowering a common limiting energy barrier. The fact that this barrier controls the permeation rate of both internal and external Mg^{2+} is difficult to reconcile with a simple view of the energy profile of the NMDA channel, which assumes two barriers and one well and in which the high barrier limiting Mg^{2+} permeation would have to be close to the internal surface. In many ways, our results are more consistent (for Mg^{2+} at least) with an energy profile in which a central barrier separates the two binding sites of external and internal Mg^{2+} (7, 35).

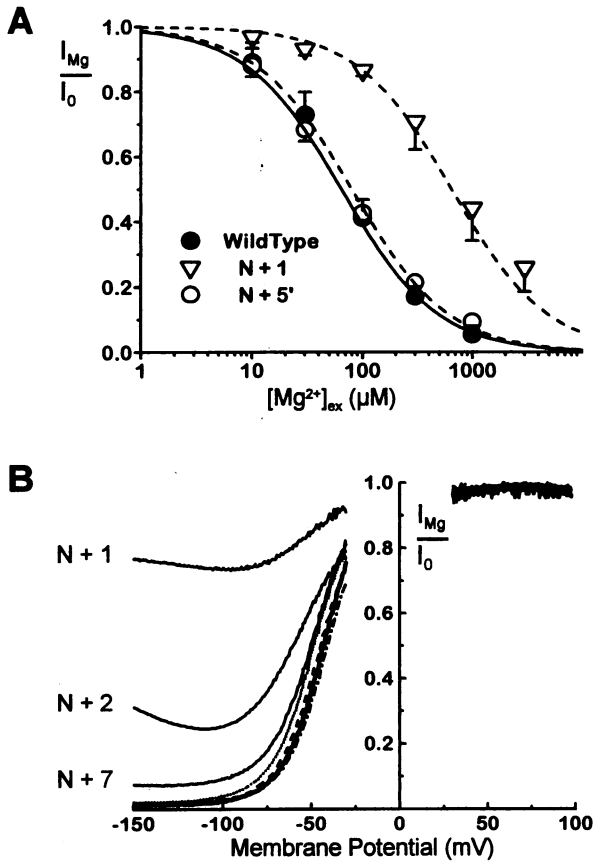

FIG. 4. Concentration and voltage dependence of external Mg^{2+} block of wild-type and mutant NMDA channels. (*A*) Inhibition curves for the wild-type, the N+1, and the N+5′ mutant channels at −50 mV. The ratio of the whole oocyte currents recorded in the presence of external Mg^{2+} over the currents recorded in the absence of external Mg^{2+} is plotted as a function of the external Mg^{2+} concentration. Data points and error bars correspond to the mean and standard deviation of measurements in at least three oocytes for each channel construct. They were fitted with the equation

$$I_{Mg}/I_0 = IC_{50}/(IC_{50} + [Mg^{2+}]_{ex}).$$

IC_{50} values of all studied channel constructs are listed in Table 1. (*B*) For each channel construct, the ratio I_{Mg}/I_0 as a function of the membrane potential is shown. Curves are obtained by dividing the *I–V* relation in the presence of 100 μM external Mg^{2+} by the *I–V* relation obtained in the absence of external Mg^{2+}. The upper three traces correspond to the mutants as indicated, the remaining four traces correspond to wild-type (thick line), N+5 (–•–•), N+5′ (– – – –), and N+6 (••••).

We thank Stéphane Supplisson for devising and constructing the modified expression plasmids, Dr. John Dempster for the STRATHCLYDE ELECTROPHYSIOLOGY software package, and Prof. Serge Hazout for advice on statistical tests. We also thank Michael Häusser, Pierre Paoletti, and Ralf Schneggenburger for critical comments on the manuscript. This work was supported by a fellowship from the Human Frontier Science Program (J.K.) and by the European Community Grant BIO 2-CT93-0243.

1. McBain, C. J. & Mayer, M. L. (1994) *Physiol. Rev.* **74**, 723–760.
2. Nowak, L., Bregestovski, P., Ascher, P., Herbet, A. & Prochiantz, A. (1984) *Nature (London)* **307**, 462–465.

3. Mayer, M. L., Westbrook, G. L. & Guthrie, P. B. (1984) *Nature (London)* **309,** 261–263.
4. Ascher, P. & Nowak, L. (1988) *J. Physiol. (London)* **399,** 247–266.
5. Jahr, C. E. & Stevens, C. F. (1990) *J. Neurosci.* **10,** 3178–3182.
6. Johnson, J. W. & Ascher, P. (1990) *Biophys. J.* **57,** 1085–1090.
7. Li-Smerin, Y. & Johnson, J. W. (1996) *J. Physiol. (London)* **491,** 121–135.
8. Moriyoshi, K., Masu, M., Ishii, T., Shigemoto, R., Mizuno, N. & Nakanishi, S. (1991) *Nature (London)* **354,** 31–37.
9. Monyer, H., Sprengel, R., Schoepfer, R., Herb, A., Higuchi, M., Lomeli, H., Sakmann, B. & Seeburg, P. H. (1992) *Science* **256,** 1217–1221.
10. Hollmann, M. & Heinemann, S. (1994) *Annu. Rev. Neurosci.* **17,** 31–108.
11. Burnashev, N., Schoepfer, R., Monyer, H., Ruppersberg, J. P., Gunther, W. & Sakmann, B. (1992) *Science* **257,** 1415–1419.
12. Mori, H., Masaki, H., Yamakura, T. & Mishina, M. (1992) *Nature (London)* **358,** 673–675.
13. Sakurada, K., Masu, M. & Nakanishi, S. (1993) *J. Biol. Chem.* **268,** 410–415.
14. Hollmann, M., Maron, C. & Heinemann, S. (1994) *Neuron* **13,** 1331–1343.
15. Stern-Bach, Y., Bettler, B., Hartley, M., Sheppard, P. O., O'Hara, P. J. & Heinemann, S. F. (1994) *Neuron* **13,** 1345–1357.
16. Wo, Z. G. & Oswald, R. E. (1994) *Proc. Natl. Acad. Sci. USA* **91,** 7154–7158.
17. Bennett, J. A. & Dingledine, R. (1995) *Neuron* **14,** 373–384.
18. Yellen, G., Jurman, M. E., Abramson, T. & MacKinnon, R. (1991) *Science* **251,** 939–942.
19. Jobling, S. A. & Gehrke, L. (1987) *Nature (London)* **325,** 622–625.
20. Kunkel, T. A. (1985) *Proc. Natl. Acad. Sci. USA* **82,** 488–492.
21. Paoletti, P., Neyton, J. & Ascher, P. (1995) *Neuron* **15,** 1109–1120.
22. Li-Smerin, Y. & Johnson, J. W. (1996) *J. Physiol. (London)* **491,** 137–150.
23. Schoenmakers, T. J., Visser, G. J., Flik, G. & Theuvenet, A. P. (1992) *BioTechniques* **12,** 870–874.
24. Johnson, J. W. & Ascher, P. (1992) *J. Physiol. (London)* **455,** 339–365.
25. Braddick, H. J. J. (1954) *The Physics of Experimental Methods* (Chapman & Hall, London), p. 21.
26. Miledi, R. (1983) *Proc. R. Soc. London B* **215,** 492–497.
27. Arellano, R. O., Woodward, R. M. & Miledi, R. (1995) *J. Physiol. (London)* **484,** 593–604.
28. Dingledine, R., Hume, R. I. & Heinemann, S. F. (1992) *J. Neurosci.* **12,** 4080–4087.
29. Ruppersberg, J. P., von Kitzing, E. & Schoepfer, R. (1994) *Semin. Neurosci.* **6,** 87–96.
30. Woodhull, A. M. (1973) *J. Gen. Physiol.* **61,** 687–708.
31. McLaughlin, S. (1989) *Annu. Rev. Biophys. Biophys. Chem.* **18,** 113–136.
32. MacKinnon, R., Latorre, R. & Miller, C. (1989) *Biochemistry* **28,** 8092–8099.
33. Lu, Z. & MacKinnon, R. (1994) *Nature (London)* **371,** 243–246.
34. Mayer, M. L. & Westbrook, G. L. (1987) *J. Physiol. (London)* **394,** 501–527.
35. Zarei, M. M. & Dani, J. A. (1995) *J. Neurosci.* **15,** 1446–1454.